NJC

Accepted Manuscript

ROYAL SOCIETY OF CHEMISTRY

www.rsc.org/njc
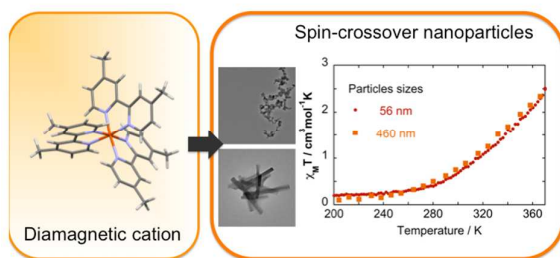
Nano- and microparticles or polycrystalline powders of the $Fe(Me_2-bpy)_2(NCSe)_2$ spin-crossover complex were easily elaborated from the diamagnetic precursor $[Fe(Me_2-bpy)_3](NCSe)_2.S$ by precipitation in an anti-solvent or by solid-state thermolysis.

Journal Name

ARTICLE

Fe(Me2-bpy)2(NCSe)2 spin-crossover micro- and nanoparticles showing a spin-state switching above 250 K.

Luong Lam Nguyen,[a] Régis Guillot,[a] Jérôme Laisney,[a] Lionel Rechignat,[b] Salma Bedoui,[b] Gabor Molnár,[b] Eric Rivière[a] and Marie-Laure Boillot[*][a]

We present the study of nano- and microparticles of the $Fe(Me_2-bpy)_2(NCSe)_2$ spin-crossover complex prepared from the diamagnetic precursor $[Fe(Me_2-bpy)_3](NCSe)_2.S$. Two solvates of the latter were characterized by single-crystal X-ray structures at 100 K (S = 2MeOH or $3H_2O$). The extraction of one Me_2-bpy per metal ion in $[Fe(Me_2-bpy)_3](NCSe)_2.S$ was achieved either by thermolysis at temperature higher than 150 °C or by precipitation in an anti-solvent, leading to a polycrystalline or particulate powder of $Fe(Me_2-bpy)_2(NCSe)_2$. This chemical conversion was investigated with TGA, powder X-ray diffraction, IR, Raman and magnetic measurements. The S=0 ↔ S=2 spin-crossover of $Fe(Me_2-bpy)_2(NCSe)_2$ centered at *ca.* 340 K is almost complete at low temperature (HS residue ≤ 5 % below 250 K) while at 370 K, the HS fraction can be estimated at ∼ 0.7. These features are essentially preserved whatever the size of particles (56, 460 and 1200 nm) as a consequence of the weak cooperativity of the process occurring at high temperature and the molecular nature of particles. This approach leading to a dispersion of small particles in a polymer suits for the preparation of materials of optical quality, *via* the stabilization and processing of nanoparticles in convenient matrices to form thin film.

Introduction

The spin-crossover materials form a class of switchable molecular materials whose transformation under external stimuli produces major changes of spin state-dependent and structural properties.[1] These features related to the vibronic nature of the process, may give rise to cooperative and hysteretic transitions at temperatures close to the ambient one, a behavior that confer to the materials interesting potentialities for technological applications.[2] Accordingly, considerable research efforts devoted to the elaboration of bistable spin transition materials, and subsequent downsizing and processing have been achieved in the last decade. It has been shown that the ability to switch such materials over a range of temperature between two stable (or metastable) spin states was preserved down to a typical size of 4 nm, 10 nm or 30 nm, depending on the chemical nature of compounds (and strength of cooperative elastic interactions, stiffness and environments of particles).[3]

The spin-state switching can be controlled by light. At low temperature, the light-induced excited spin state trapping (LIESST) allows achieving a bistability between the photoinduced metastable HS state and the LS ground state for a number of Fe^{II} compounds.[4] Such solid-state transformations were performed with poorly absorbing samples, i.e. either very thin (or highly doped) single-crystals or small amounts of powder. The synthesis of nanosized molecular solids appears as a key feature for the investigation of the photoswitching properties (mechanism, dynamic) in the solid-state and for elaborating devices.[5,6,7]

We report here the study of a $Fe(Me_2-bpy)_2(NCSe)_2$ compound that may be easily functionalized with various substituents. For this investigation, we have revisited the preparation of $Fe(Me_2-bpy)_2(NCSe)_2$,[8] from a parent compound[9] $[Fe(Me_2-bpy)_3](NCSe)_2.3H_2O$ which remains diamagnetic at any temperature and may be precipitated in the form of particles in presence of an anti-solvent.[10] We have investigated the chemical nature of these particles, their physical properties from magnetic, optical, vibrational measurements and then discussed the observations with respect to literature.

Experimental

CHEMICAL SYNTHESES

4, 4'-dimethyl-2,2'-bipyridine (Aldrich, 99%), potassium selenocyanate (Aldrich, 99%) were used without further

purification. The synthesis of the Fe(II) complex was performed under an argon atmosphere, using previously degassed solvents.

[Fe^{II}(Me$_2$-bpy)$_3$](NCSe)$_2$.3H$_2$O. A solution of Fe(SO$_4$)$_2$(NH$_4$)$_2$.6H$_2$O (142 mg, 0.36 mmol) in water (5 mL) was added dropwise to a methanolic solution (5 mL) of Me$_2$bpy (200 mg, 1.086 mmol) which was previously heated to 50 °C. The red mixture was stirred at 50 °C for 1 hour, then cooled to room temperature. A saturated solution of KNCSe (1g, 6.9 mmol) in water was slowly added to the Fe(II) salt, the mixture was stirred for 20 min and decanted. The dark red solid was collected by filtration and dried under argon. Single-crystals were isolated by slow evaporation of methanolic solution of this salt. Depending on the amount of water in this solution, single-crystals of H$_2$O (platelet) or CH$_3$OH (square-shaped) solvates were formed and characterized by single-crystal X-ray diffraction measurements.

Elemental analysis: formula for n=3 water molecules C$_{38}$H$_{42}$FeN$_8$O$_3$Se$_2$ (MM 874.11 gmol^{-1}) Calcd (%): C 52.31, H 4.85, N 12.84; Found (%): C 52.63, H 4.76, N 12.86; EDS analysis Fe/Se = 1/2; IR (KBr): ν= 2061 cm^{-1}(NC$_{NCSe}$).

Thermogravimetric analysis. The thermogram shows an immediate loss of weight with a plateau around 100 °C (found 5.7 %, calcd for three water molecules 6.2 %). A new step clearly appears at 175 °C that corresponds to the removal of one bidentate ligand per formula (found for the total variation of weight 27.5 %, calcd for one Me$_2$bpy and three H$_2$O molecules 27.2 %).

Fe^{II}(Me$_2$-bpy)$_2$(NCSe)$_2$. This compound was first prepared by a solid-state synthesis that was mentioned in reference 11 for an analogue Fe(phen)$_2$(NCS)$_2$. According to the previous analysis, the polycrystalline powder of [Fe^{II}(Me$_2$-bpy)$_3$] (NCSe)$_2$ was heated at 175 °C for 4 hours (with/without vacuum). The purple polycrystalline powder was collected and characterized.

Elemental analysis: formula C$_{26}$H$_{24}$FeN$_6$Se$_2$ (MM 635.97 gmol^{-1}) Calcd (%): C 49.23, H 3.81, N 13.25; Found (%): C 49.99, H 3.83, N 12.89; EDS analysis Fe/Se = 1/1.84. IR(KBr): ν= 2061, 2070 cm^{-1} (NC$_{NCSe}$), ν= 2098, 2103 (shoulder) cm^{-1}(NC$_{NCSe}$).

1.2 μm microparticles of **Fe^{II}(Me$_2$-bpy)$_2$(NCSe)$_2$** were prepared by an alternative method for extracting the bidentate ligand. It consists to dissolve 10 mg of [Fe^{II}(Me$_2$-bpy)$_3$](NCSe)$_2$.3H$_2$O in 1 mL of Ethanol. The red solution rapidly evolves and forms a suspension of violet microcrystalline powder that was isolated by centrifugation (9000 rpm, 10 min) after the addition of 10 mL of butanol, then was rinsed with pentane and dried.

Elemental analysis: formula C$_{26}$H$_{24}$FeN$_6$Se$_2$ (MM 635.97 gmol^{-1}) Calcd (%): C 49.23, H 3.81, N 13.25, Fe 8.80, Se 24.90; Found (%): C 49.44, H 3.87, N 13.06, Fe 8.94, Se 24.14; EDS analysis Fe/Se = 1/2. IR(KBr): ν= 2061, 2070 cm^{-1}(NC$_{NCSe}$), ν= 2098, 2103 (shoulder) cm^{-1}(NC$_{NCSe}$).

The sudden precipitation approach was applied for controlling the nucleation and growth of small particles in an anti-solvent.[10]

460 nm nanoparticles of **Fe^{II}(Me$_2$-bpy)$_2$(NCSe)$_2$.** 10 mg of the cationic complex dissolved in 2 mL of ethanol were quickly added to a previously heated (65 °C) volume of toluene (20 mL) in which 200 mg of PMMA (poly(methyl methacrylate), PMMA

15000 or 35000) were dissolved. The mixture was vigorously stirred for 15 min, then the mixture was centrifugated for 10 min (at 10 000 rpm). The light purple solid was filtered, rinsed with pentane, centrifugated. These last steps were repeated before drying under vacuum powder.

56 nm nanoparticles of **Fe^{II}(Me$_2$-bpy)$_2$(NCSe)$_2$.** The previous synthesis was carried out in the same conditions but here the 500 nm objects were removed with a 0.2 mm PTFE membrane just after the step of heating and stirring of the mixture. The filtrate was centrifugated.

CRISTALLOGRAPHY

The single-crystal X-ray diffraction data were collected by using a Kappa X8 APPEX II Bruker diffractometer with graphite-monochromated Mo$_{K\alpha}$ radiation (λ = 0.71073 Å). At 100 K: the crystal was mounted on a CryoLoop (Hampton Research) with Paratone-N (Hampton Research) as cryoprotectant and then flashfrozen in a nitrogen-gas stream at 100 K. The temperature of the crystal was maintained at the selected value by means of a 700 series Cryostream cooling device within an accuracy of ±1 K. The data were corrected for Lorentz polarization, and absorption effects. The structures were solved by direct methods using SHELXS-97[12] and refined against F^2 by full-matrix least-squares techniques using SHELXL-97[13] with anisotropic displacement parameters for all non-hydrogen atoms. Hydrogen atoms were located on a difference Fourier map and introduced into the calculations as a riding model with isotropic thermal parameters. All calculations were performed by using the Crystal Structure crystallographic software package WINGX.[14] CCDC 1010286 and 1010287 (corresponding to [Fe^{II}(Me$_2$-bpy)$_3$](NCSe)$_2$.S with S = 2CH$_3$OH and 3H$_2$O) contains the supplementary crystallographic data for this paper. These data can be obtained free of charge at www.ccdc.cam.ac.uk/conts/retreving.html or from the Cambridge Crystallographic Data Center, 12 union Road, Cambridge CB2 1EZ, UK; Fax: (internat.) + 44-1223-336-033; E-mail: deposit@ccdc.cam.ac.uk].

PHYSICAL MEASUREMENTS

Thermal gravimetric analysis

The measurement was done under ambient atmosphere with a TGA analyser (TA intruments-water LLC, SDT Q600) in the 293 - 473 K temperature range at a rate of 2°C per min.

FTIR measurements

The spectra were collected on KBr pellets at room temperature with a Perkin-Elmer spectrometer (Spectrum 100).

Powder X-ray diffraction measurements

The XRD patterns were recorded at room temperature on powders deposited on aluminium plate, using a Philipps Panalytical X'Pert Pro MPD powder diffractomer at CuKα radiation equipped with a fast detector within the 6 - 35° 2θ range.

TEM measurements

The TEM images were acquired with a TEM JEOL 1400 (120 kV)Z equipped two high-resolution and high-speed digital CCD Gatan camera.

Magnetic measurements

Magnetic measurements were carried out using a Quantum Design SQUID magnetometer (MPMS5S Model) calibrated against a standard palladium sample. The data were collected between 100 and 370 K at a rate of 2 K min^{-1}.

Optical microscopy measurements

The crystals were enclosed in a Linkam THMS600 heating-cooling stage and optical microscopy images of the crystals were recorded either isothermally or during a temperature rise (1 K/min) using an Olympus BX51 microscope equipped with a 20X objective and a color CCD camera (Motic). The sample was illuminated by a halogen lamp (400–700 nm) in transmission mode.

Raman Measurements

Variable temperature Raman spectra were recorded using a Labram-HR (Jobin-Yvon) microspectrometer and a liquid-nitrogen cryostage (Linkam THMS 600). The 632.8 nm line of a He-Ne laser (17 mW) was used as the excitation source and the laser heating effects of the sample were minimized by additional filters (OD = 2-3) on the excitation beam. Owing to the micro-/nano-crystalline nature of the samples laser polarization effects were not investigated in more detail.

Results

We have considered the ionic complex and its conversion into the neutral spin-crossover analogue. Two synthetic routes were examined: first, the solid-state reactivity of the precursor at high temperature that provided a polycrystalline material, then a solvent-assisted precipitation method leading to size-reduced molecular materials whose properties were investigated and discussed with respect to those of bulk.

Characterization of the precursor

X-ray structure analysis

Single-crystals of [Fe(Me$_2$-bpy)$_3$](NCSe)$_2$.3H$_2$O were easily isolated from crystallogeneses in methanol in the presence of traces of water. The crystalline structures show variable packing involving the salt and water molecules with only minor changes in the cation (Tables ST1, ST2 in ESI). We focus here on the compound of formula [Fe(Me$_2$-bpy)$_3$](NCSe)$_2$.2CH$_3$OH which appears to have the best crystalline quality. This solvate was obtained as dark red single-crystals by slow evaporation of a methanolic solution. It crystallizes in the triclinic P$\bar{1}$ space group and its structure collected at 100 K consists of cationic complexes, NCSe$^-$ anions and methanol molecules. Crystal data collection and refinement parameters are described in Table 1. Selected bond lengths and molecular parameters are displayed in Table 2.
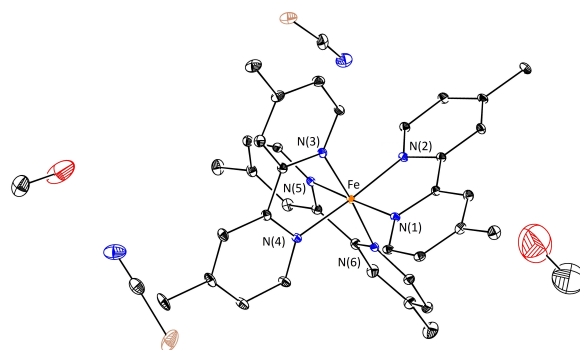

Figure 1: ORTEP view of the asymmetric unit of [Fe(Me$_2$-bpy)$_3$](NCSe)$_2$.2CH$_3$OH at 100 K with ellipsoids cut at the 30% probability level. Hydrogen atoms are omitted for clarity.

In Figure 1, the molecular structure of the cation shows an Fe^{II} ion in the [N$_6$] environment of three bidentate ligands. Average bond lengths, Σ and ζ parameters (see caption of Table 2) are typical for a low-spin Fe^{II} ion and fully compare with values reported for the [Fe(Me$_2$-bpy)$_3$](NCS)$_2$.3H$_2$O analogue (<Fe-N> = 1.965(3) Å, Σ = 62.9°, ζ = 0.024 Å respectively).[15]
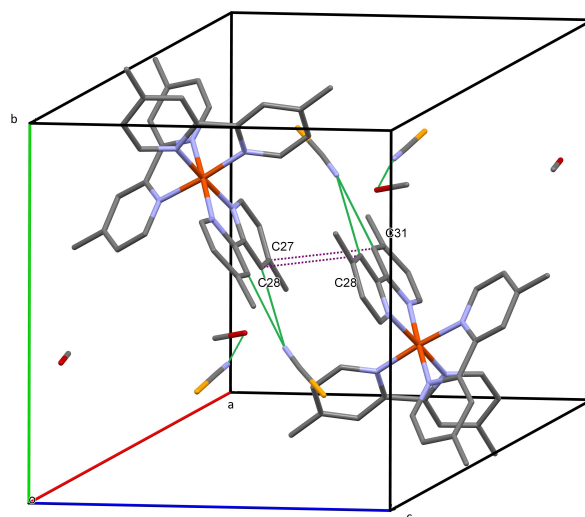

Figure 2: Packing of [Fe(Me$_2$-bpy)$_3$](NCSe)$_2$.2CH$_3$OH at 100 K showing the shortest inter-ring distances as well as the close contacts between NCSe anions and carbon atoms of methanol or aromatic groups.

In Figure 2, the complexes related by the inversion centre form dimers with bipyridine ligands of two adjacent sites lying in almost parallel planes (inter-ring C-C distances at 3.769 and 3.885 Å for C28-C28 and C27-C31, respectively). The NCSe$^-$ anions are involved in short Van der Waals contacts between the N atoms and the H-C groups (in ortho or meta position) of bpy rings or the H-O group of methanol.

The arrangement of dimers is stabilized via numerous and moderate contacts located in planes parallel to *bc*; weaker interactions being observed in-between the planes. Finally even

at 100 K, the disorder of atomic position remains marked for the N and O atoms of methanol molecules as well as for the $NCSe^-$ anion that interacts only with the solvent.

Table 1 Crystal data and structure refinement for $[Fe^{II}(Me_2\text{-}bpy)_3](NCSe)_2.2CH_3OH$ at 100 K.

Compound and Temperature	$[Fe^{II}(Me_2\text{-}bpy)_3](NCSe)_2.2CH_3OH$ 100 K
Empirical formula	$C_{40} H_{44} Fe N_8 O_2 Se_2$
Formula weight	882.60
Crystal system	triclinic
Space group	$P\bar{1}$
a (Å)	10.594(1)
b (Å)	14.297(1)
c (Å)	14.518(1)
α (°)	84.866(1)
β (°)	68.830(1)
γ (°)	77.339(1)
V (Å^3)	2000.5(2)
Z	2
Density (calc.) (g.cm^{-3})	1.465
$F(000)$	900
θ range (°)	1.46 - 36.42
Collected data	36266
Unique data	16446
R_{int}	0.0262
Data($I > 2\sigma(I)$)/restraints/parameters	11527/0/488
Goodness-of-fit on F^2	1.035
$R1 [I > 2\sigma(I)]$	0.0632
$wR2 [I > 2\sigma(I)]$	0.1633
$R1$ (all data)	0.0978
$wR2$ (all data)	0.1832

Table 2 The geometry of the Fe site surroundings.

	100 K
Fe-N bonds (Å)	
Fe-N1	1.959(2)
Fe-N2	1.960(2)
Fe-N3	1.974(2)
Fe-N4	1.974(2)
Fe-N5	1.965(2)
Fe-N6	1.968(2)
<Fe-N>	1.967(2)
ζ (Å)^a	0.032
Σ (°)^a	52.5

$$\langle Fe - N \rangle = \frac{1}{6}\sum_{i=1}^{6} d_{Fe-N_i} \quad \zeta = \sum_{i=1}^{6}|Fe - L_i - <Fe - L>| \quad \Sigma = \sum_{i=1}^{12}|90 - \phi_i|$$

TGA analysis.

Heating the red polycrystalline powder (Fig. 3) leads to the removal of three water molecules (plateau at ca. 115 °C). Between 140 and ca 175 °C, a new variation of weight corresponds to the removal of one Me_2-bpy ligand per formula unit, as confirmed by the elemental analysis of the purple powder (see below).
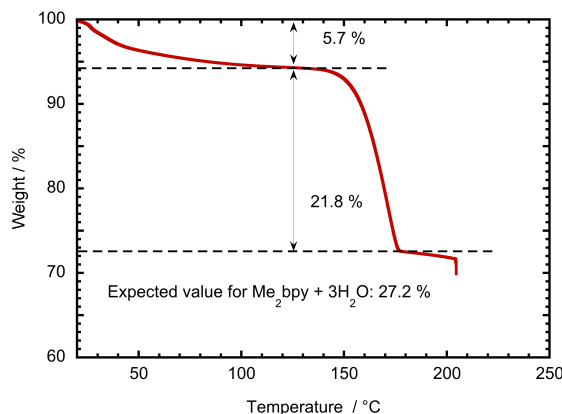
Observation of crystals upon the thermal evolution

This thermal reactivity was monitored between 107 and 204 °C with optical microscopy by recording images of both $[Fe(Me_2\text{-}bpy)_3](NCSe)_2$ solvates (Solvent = CH_3OH or H_2O) in the crystalline form.

Figure 3: TGA analysis of $[Fe(Me_2\text{-}bpy)_3](NCSe)_2.3H_2O$ performed at 2°C / min under air atmosphere

Figure 4a shows the 160 °C isothermal evolution of the red square-shaped methanolate sample. The image selected at an 11 min reaction time indicates the formation of a number of stripes parallel to the left edge of the crystal, then later the crystal color strongly darkens and the macroscopic change of volume becomes apparent. The transformation achieved after 100 min essentially preserves the shape of the solid (linear variation of edges size and angle, Fig. S1 in ESI).
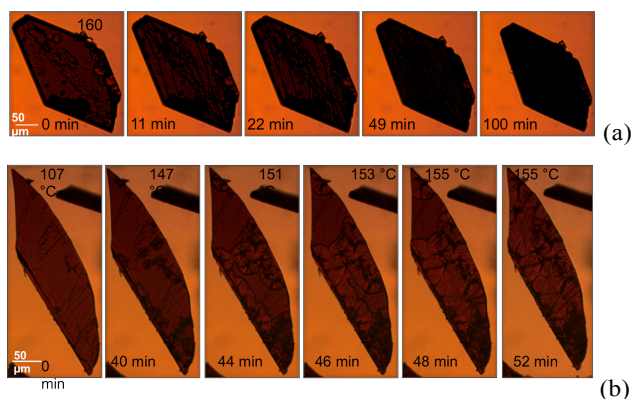

Figure 4: Optical microscopy images of $[Fe(Me_2\text{-}bpy)_3](NCSe)_2$. S (S = CH_3OH or H_2O) after the desolvatation stage: (a) the 160 °C isothermal evolution of the red square-shaped methanolate sample; (b) evolution of the initially hydrated sample upon heating from 107 to 155 °C (scanning rate of 1°C/min) and then staying at 155 °C.

Figure 4b presents the evolution with temperature of the platelets of hydrated compound. The sequence starts with the dehydrated material at 107 °C, that was heated to 155 °C (scanning rate = 1 °C/min), temperature at which the variation was stopped for studying the stage corresponding to the ligand release. A number of flower-type patterns emerge close to the

crystal edges or to the areas rich in crystalline defects and then, growth in a concentric manner and coalesce in the whole volume. The solid deformation also appears through the proliferation of defects in between crystalline fragments and the change of crystal dimensions (video available in the SI) and volume.

Synthesis of $Fe^{II}(Me_2\text{-bpy})_2(NCSe)_2$

The polycrystalline powder. $Fe^{II}(Me_2\text{-bpy})_2(NCSe)_2$ was prepared according to an uncommon solvent-free approach[11,16] that was early mentioned in the reports on $Fe^{II}(phen)_2(NCS)_2$ syntheses. It was optimized from the thermal behavior of the cationic precursor as determined above.

The X-ray diffractograms 293 K of the powder of precursor, before and after the thermal reaction are superimposed in Figure 5. The disappearance of Bragg reflections specific to the cationic precursor (2θ = 6.6, 9.9, 12.7 and 30.8 °) and the appearance of new sharp Bragg reflections (8.5, 12.2, 18.7 and 21.9°) indicate the complete transformation of the former as well as the crystallinity of the product.
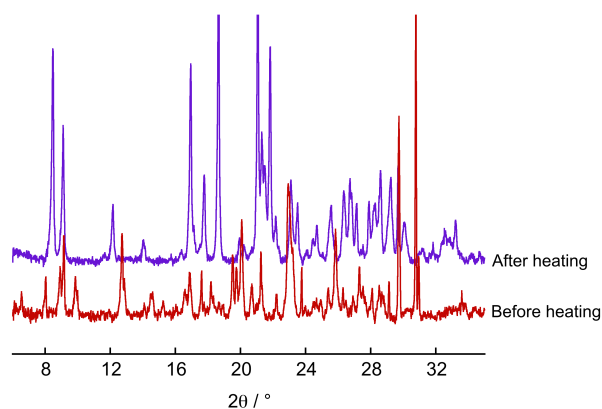

Fig. 5: X-ray diffractograms of the powder of precursor recorded at 293 K, before and after the thermal reaction(175 °C, 4 hours, vacuum).

The comparison of the two IR spectra recorded at T = 293 K (Fig. S2) confirms the drastic change of the coordination sphere around the metal ion. The well-known band near 2100 cm^{-1} associated to the NC stretching mode of NCSe$^-$ is centred at 2061 ± 4 cm^{-1} for the [Fe(Me$_2$-bpy)$_3$](NCSe)$_2$.3H$_2$O salt. After the thermal treatment, the two double bands (2061 and 2070 ± 4 cm^{-1}, 2098 and ~2103 ± 4 cm^{-1}) are typical of *cis* positioned NCSe ligands, N-coordinated to a HS and LS Fe^{II} ion, respectively.[16,17,18,19] The molecular rearrangement also gives rise to changes of intensity and splitting of bands, and to the appearance in the low frequency range of new vibrational frequencies (419, 515, 630 and 845 ± 4 cm^{-1}).

We can infer from the TGA, powder X-ray, IR measurements and the color change that the thermal decomposition of the cationic precursor in the present conditions results in the formation of a polycrystalline powder of Fe^{II}(Me$_2$-bpy)$_2$(NCSe)$_2$. The fact that two NCSe stretching modes, separated by 35-40 cm^{-1}, can be observed by IR spectroscopy

suggests the coexistence in this solid of HS and LS Fe^{II} complexes at room temperature. This will be further examined by magnetic measurement (see below).

Micro- and nanocrystals. The compound was prepared in the form of particles by using the dissociative equilibrium between the cationic species and the poorly soluble complex Fe^{II}(Me$_2$-bpy)$_2$(NCSe)$_2$.[16] With polar solvents (EtOH) and concentrated solution (11.3 mM) of the red iron(II) salt, we have first observed the spontaneous precipitation of purple particles. The TEM image of these particles (Fig. 6a) indicates the formation of very thin needle-like objects whose size varies between 1 and 5 μm depending on the temperature (T = 65 and 80°C, respectively).

The combination of dilution, change of reaction temperature and fast precipitation in an antisolvent (in presence of a confining polymer, here PMMA) has allowed us to isolate smaller objects. It appears from TEM measurements (Fig. 6b) that 460(190)x80(30) nm^2 platelets and 56(15) nm (Fig. S3) spherical particles coexist in the ethanol-toluene mixture maintained a 65 °C. A last step of filtration affords the smallest particles (56 ± 15 nm, Fig. 6c).

(a) (1200 ± 200) x (500 ± 65) nm^2 microparticles
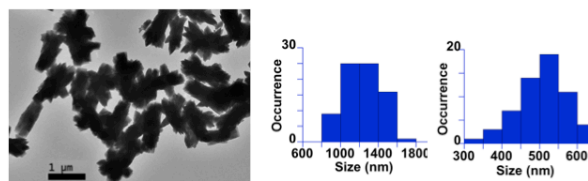
(b) (460 ± 190) x (80±30) nm^2 nanoparticles
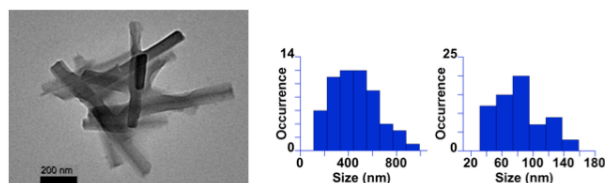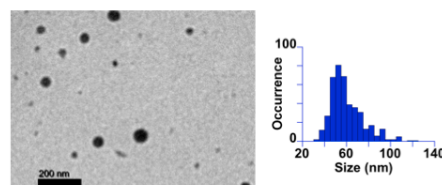

(c) 56 ± 15 nm nanoparticles

Fig.6: TEM images showing the particles that (a) spontaneously precipitate from a concentrated ethanolic solution of cationic precursor, (b) and (c) precipitate by sudden addition of the ethanolic solution of precursor in toluene (see the text), and their size dispersion (long and short edges for a and b, diameter for c).
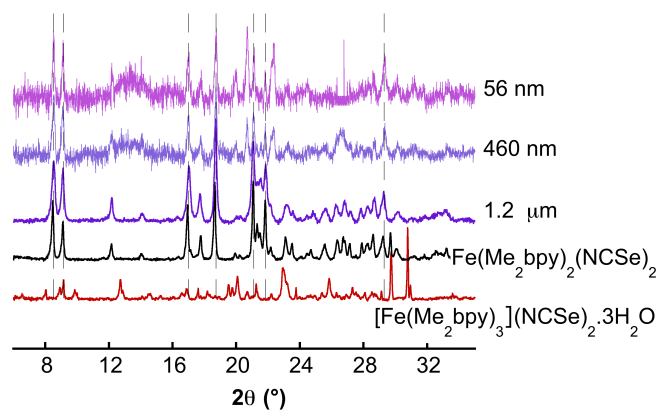
Fig. 7: Powder X-ray diffractograms at 293 K: samples of precursor before and after thermal treatment, microcrystals (1.2(0.2)x0.5(0.065) μm^2), nanoparticles (460(190)x80(30) nm^2 and 56(15) nm) both being dispersed in PMMA. A few extra peaks (*19.93, 20.62, 22.29, 24.44, 26.45) are due to the Al substrate of the sample.

We have observed that the 56 nm particles of the neutral species were exclusively formed if the volume of ethanol was increased (from 2 to 5 mL) all else being equal (volume of toluene, temperature, addition of PMMA, reaction time). These features can be related to the fact that the formation of particles is not straightforward and depends on the kinetics of ligand extraction and of precipitation.

The corresponding X-ray diffractograms recorded at room temperature are displayed in Figure 7. Comparison with those recorded before and after heating the cationic precursor provides evidences for the formation of $Fe^{II}(Me_2\text{-bpy})_2(NCSe)_2$ in the form of crystalline micro- and nanoparticles. Therefore the nature and crystallinity of the solid phase of $Fe^{II}(Me_2\text{-bpy})_2(NCSe)_2$ are preserved regardless of the chemical approach used for the synthesis.
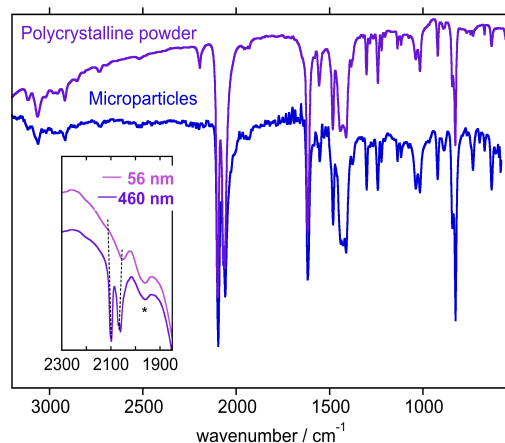

Fig. 8: 293 K IR spectra of samples of precursor after thermal treatment, of microcrystals (1.2(0.2)x0.5(0.065) μm^2) and in the inset, an expansion of spectra showing the NC stretching vibrational mode for the dispersion of nanoparticles (460(190)x80(30) nm^2 and 56(15) nm) in PMMA. All the samples were in the form of KBr pellets.

The spectroscopic characterization of microcrystals by IR (in Fig. 8) is in agreement with the features above mentioned for $Fe^{II}(Me_2\text{-bpy})_2(NCSe)_2$. No trace of the Me_2-bpy base-free ligand can be detected, in particular near 1600 cm^{-1} in the range of the N=C stretching mode. The isolation of nanoparticles embedded in an excess of PMMA gives rise to strong absorption bands (for example due to the ester functions) of the polymer that prevents the analysis of the molecular spectrum except the two vibrational modes associated to the coordinated NCSe ligands in the 2000-2150 cm^{-1} range (see inset in Figure 8). This feature supports the analysis of powder X-ray diffraction data indicating the formation of micro- and nanocrystals of the neutral compound.

Magnetic measurements

Magnetic measurements were carried out as a function of temperature between 100 and 370 K. This latter value was fixed slightly below the glass transition of PMMA (at ca. 380 K) in which the particles were dispersed in order to minimize a matrix effect on the samples.[20] It was first checked that the powder of $[Fe(Me_2\text{-bpy})_3](NCSe)_2.3H_2O$ is fully diamagnetic at room temperature ($\chi_M T \sim 0$ $cm^3 mol^{-1}K$, χ_M being the molar magnetic susceptibility), a result consistent with the strong ligand-field strength produced by diimine ligands.[1,9]

The Fig. 9 shows the temperature dependence of the $\chi_M T$ product of $Fe^{II}(Me_2\text{-bpy})_2(NCSe)_2$ in the form of polycrystalline (bulk) sample. The S=0 ↔S=2 spin-crossover observed above 250 K, is still uncompleted at 370 K as the $\chi_M T$ value at 2.57 $cm^3 mol^{-1}K$ (371 K) correspond to a fraction of HS species $\gamma_{HS}=$ ca. 0.7 (with $\chi_M T = 3.50$ $cm^3 mol^{-1}K$ for a pure HS species, value extrapolated from the data in reference 8). At 100 K, the value of $\chi_M T = 0.10$ $cm^3 mol^{-1}K$ suggests the presence of traces of HS residue ($\gamma_{HS}^{residue} < 5\%$). This curve is in agreement with the properties of $Fe^{II}(Me_2\text{-bpy})_2(NCSe)_2$ prepared by refluxing an hydrated salt in aromatic solvents (see comparison in Fig. S4).[8]

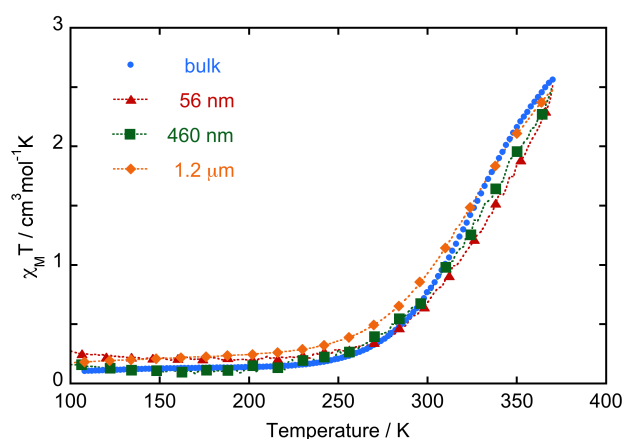Fig. 9: Temperature dependence of $\chi_M T$ for $Fe^{II}(Me_2\text{-bpy})_2(NCSe)_2$ in the form of a polycrystalline powder (●), microparticles (◆) and in-PMMA nanoparticles (■, 460(190)x80(30) nm^2) or (▲, 56(15) nm).

An estimate of the temperature corresponding to a half-complete transition is $T_{1/2} \sim 340$ K. The fact that the fraction of LS species at 300 K is still larger than the HS one ($\gamma_{HS} = 0.22$, here including the residue) is consistent with the IR data showing two NC_{NCSe} modes with a prevailing component at ca. 2100 cm^{-1}. As expected for a progressive transformation with a poor cooperative character, the behaviour of micro- and nanocrystalline samples satisfyingly matches the one observed for the bulk and thus is preserved whatever the particles sizes.

Raman measurements,

The previous data were completed by Raman measurements, which allow the spectral identification of the HS and LS species, even in the presence of PMMA, and the extraction of the fraction of spin-crossover species as a function of temperature. The spectra of all the samples were collected with a 632.8 nm excitation wavelength at different temperatures (200, 300 and 370 K). The characterization of the bulk sample confirms the thermal reaction that is previously discussed and provides the frequencies characterizing both forms (Fig. S5). All the spectra observed at a fixed temperature, for $Fe^{II}(Me_2\text{-bpy})_2(NCSe)_2$ in the form of bulk, micro- and nanoparticles (Fig. S6, Table ST3) are qualitatively comparable. Figure 10 shows the spectral evolution in the case of microparticles. The vibrational modes associated to NCSe ligands (2100, 2107 and ca. 2071, 2061 cm^{-1}) can be used as markers of LS and HS forms for analyzing the thermal spin crossover.

The relative intensity of the LS peak at the working temperatures yields a set of points that compares reasonably well to the magnetic curve (Fig. S7). The process that appears almost complete at 200 K, corresponds to a HS residue varying between ca. 5 (bulk, 460(190)x80(30) nm^2) and 17 (56(15) nm) % for the different samples.
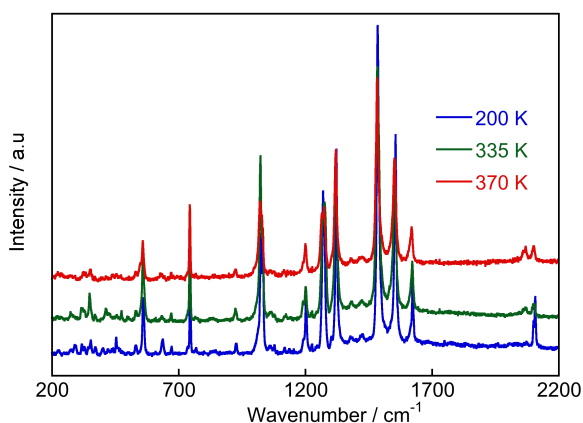

Fig. 10 Variable temperature Raman spectra collected for the 1.2 μm microparticles of $Fe^{II}(Me_2\text{-bpy})_2(NCSe)_2$.

Discussion

From a synthetic point of view, the ligand extraction from the cationic complex contributes to the shift of the chemical equilibrium towards the formation of the neutral species whereas the reverse reaction is driven by the presence of water.[21] This alternative is discarded by the solid-state synthesis that can be easily controlled for a complete transformation of the complex.

The powder X-ray diffraction data collected for $Fe^{II}(Me_2\text{-bpy})_2(NCSe)_2$ confirm the preservation of one crystalline phase whatever the method used for the removal of one bipyridine ligand (solvent-induced or solvent-free extraction). This feature is quite remarkable as the thermal switching properties of spin-crossover solids are usually modulated by subtle factors related to the solid-phase that depend on the chemical synthesis and crystallinity. The versatility of molecular organization and packing is reflected by polymorphism and variable spin-crossover behavior,[22] as nicely demonstrated in the case of $Fe(PM\text{-BiA})_2(NCS)_2$.[23]

One interesting result observed here is the formation of a crystalline material that derives from a coordination bond cleavage, diffusion of ligand in the solid state, rearrangement of the coordination sphere and nucleation of the new phase. It is well established that in contrast to the methods developed for the elaboration of oxides nanostructures,[24,25] softer thermal conditions may lead either to a molecular rearrangement *via* the migration of ligands between the coordination spheres of two metal ions,[26] or to a coordination polymer *via* a partial decomposition, a rearrangement of halide (or pseudohalide like NCX) ions to form bridges between metal ions.[27] Finally, Guionneau has identified for some particular spin-crossover materials, a relationship between the solid-state crystallinity and a thermal treatment.[22]

From the background accumulated on spin-crossover Fe^{II} materials,[28] it appears that the introduction of two diimine and pseudohalide ligands in the coordination sphere may be suitable for the achievement of a spin-state switching material. As expected for compounds exhibiting similar packing, the ligand-field strength associated to the half-conversion $T_{1/2}$ temperature is found to increase by the substitution of NCS$^-$ by NCSe$^-$,[29] or bpy by Me_2-bpy.[30] For the present compound, the LS form of the compound is observed for T ≤ 250 K.

The spin-crossover curve and temperature are preserved when the compound is prepared in the form of polycrystalline, micro- or nanocrystals, that is through a size range extending from 100's microns to 56 nm. This feature is not surprising as we consider here a thermal transformation with a too weak cooperative character[3] for observing a downsizing effect, and the crystallinity is maintained in the different molecular samples.[7]

Conclusions

We have focused on two Fe(Me$_2$-bpy)x(NCSe)$_2$ prototypical compounds that are found at room temperature either in a diamagnetic (x=3) or paramagnetic (x=2) state as a consequence of a partial spin-crossover process centered at a temperature slightly above room temperature. These complexes can be interconverted either by solid-state thermolysis or by playing with their chemical equilibrium for inducing the precipitation of the neutral species.

Micro- and nanoparticles of the spin-crossover compound have been isolated with size varying between ca. 4500 and 56 nm. The magnetic behavior is preserved whatever the particles size and the spin-crossover process is quantitative. A priori, nano-sized particles will be suitable for the preparation of materials of optical quality, via their stabilization and processing in convenient matrices to form thin films.

The fact that a spin-crossover compound may be thermally prepared from a simple and chemically stable precursor may be of interest for molecular deposition on substrates, processing in micro-, nanosized patterns or nanopores.[3,5,31,32] Indeed in absence of cooperative interactions, spin-crossover type molecules dispersed in highly diluted media present distinctive properties (chemical reactivity, spin-state switching possibly coupled to electron transfer, adduct formation and transport, IRM, …) that are currently attracting particular interest.

Finally, the present approach can be applied to molecular spin-crossover analogues, for example incorporating photoswitchable ligands as required in the so-called ligand-driven light-induced spin-change effect (LD-LISC).[33] This work on derivatives that might be switched by light around room temperature is a stage in progress that will be reported.

Acknowledgements

Notes and references

a ICMMO-ECI, UMR CNRS 8182, Université Paris-Sud, Orsay, France.
b LCC, CNRS & Université de Toulouse (UPS, INP), Toulouse, France.

Electronic Supplementary Information (ESI) available: [Crystal data and molecular geometry of [Fe(Me$_2$-bpy)$_3$](NCSe)$_2$. 3(H$_2$O) (Tables ST1, ST2), optical microscopy (Fig. S1) images, Raman data (Table ST3), powder X-ray analysis (Fig. S2), IR and Raman spectra (Fig. S3 and S6) of Fe(Me$_2$-bpy)$_x$(NCSe)$_2$ complexes (x = 2,3), TEM images (Fig. S4) and VT Raman spectra (Fig. S7) of nanoparticles, Fig. S5: comparison between literature and the χ_MT *vs.* T curve of Fe(Me$_2$-bpy)$_2$(NCSe)$_2$, Fig. S8: comparison between the HS fraction extracted from magnetic susceptility measurement and Raman data]. See DOI: 10.1039/b000000x/

1 Spin-Crossover in Transition Metal Compounds, I–III, in Topics in Current Chemistry, ed. P. Gütlich and H. A. Goodwin, Springer, Berlin, 2004, vol. 233–235., Special issue in: *Eur. J. Inorg. Chem.* **2013**, 5–6; Spin-crossover materials: *Properties and Applications* (Ed.: M. A. Halcrow), Wiley, Chichester, UK, **2013**.

2 J.-F. Létard, P. Guionneau and L. Goux-Capes, in: *Topics in Current Chemistry*, vol. 235, *Spin Crossover in Transition Metal Compounds I–III* (Eds.: P. Gütlich, H. A. Goodwin), Springer, Heidelberg, Germany, **2004**, p. 221–249.

3 A. Bousseksou, G. Molnár, L. Salmon and W. Nicolazzi, *Chem. Soc. Rev.*, 2011, **40**, 3313.

4 A. Hauser, in: *Topics in Current Chemistry*, vol. 234, *Spin Crossover in Transition Metal Compounds I–III* (Eds.: P. Gütlich, H. A. Goodwin), Springer, Heidelberg, Germany, **2004**, p. 155.

5 L. Catala, F. Volatron, D. Brinzei and T. Mallah, *Inorg. Chem.*, 2009, **48**, 8, 3360 ; S. Lepoutre, D. Grosso, C. Sanchez, G. Fornasieri, E. Rivière and A. Bleuzen, *Adv. Mater.* , 2010, **22**, 3992 ; D. M. Pajerowski, J. E. Gardner, F. A. Frye, M. J. Andrus, M. F. Dumont, E. S. Knowles, M. W. Meisel and D. W. Talham, *Chem. Mater.*, 2011, **23**, 3045.

6 H. J. Shepherd, G. Molnár, W. Nicolazzi, L. Salmon and A. Bousseksou *Eur. J. Inorg. Chem.* 2013, 653 ; A. Tissot, *New J. Chem.*, 2014, **38**, 1740.

7 P. Chakraborty, M.-L. Boillot, A. Tissot and A. Hauser, *Angew. Chem. Int. Ed.*, 2013, **52**, 7139-7142 ; R. Bertoni, M. Lorenc, A. Tissot, M. Servol, M.-L. Boillot and E. Collet, *Angew. Chem. Int. Ed.*, 2012, **51**, 7485-7489 ; G. Gallé, C. Etrillard, J. Degert, F. Guillaume, J.-F. Létard and E. Freysz *Appl. Phys. Lett.* 2013, **102**, 063302.

8 A. J. Cunningham, J. E. Ferguson, H. K. J. Powell, E. Sinn and H. Wong, *J. Chem. Soc. Dalton Trans.,* 1972, 2155-2160.

9 E. Sinn, *Inorg. Chim. Acta*, 1969, **3**, 11-16.

10 A. Tissot, L. Rechignat, A. Bousseksou and M.-L. Boillot, *J. Mater. Chem.*, 2012, **22**, 3411-3419.

11 W. A. Baker and H. M. Bobonich, *Inorg. Chem.*, 1964, **3**, 1184.

12 G.M. Sheldrick, SHELXS-97, Program for Crystal Structure Solution, University of Göttingen, Göttingen, Germany, 1997.

13 G. M. Sheldrick, SHELXL-97, Program for the refinement of crystal structures from diffraction data, University of Göttingen, Göttingen, Germany, 1997.

14 L. J. Farrugia, *J. Appl. Cryst.*, 1999, **32**, 837.

15 W. Huang and T. Ogawa, *J. Mol. Struct.*, 2006, **785**, 21.

16 E. König, *Coord. Chem. Rev.,* 1968, **3**, 471.

17 E. König and K. Madeja, *Inorg. Chem.,* 1967, **6**, 48; E. König and K. Madeja, *Spectrochimica Acta*, 1967, **23A**, 45-54.

18 M. Sorai and S. Seki, *J. Phys. Chem. Solids*, 1974, **35**, 555-570.

19 E. J. MacLean, C. M. McGrath, C. J. O'Connor, C. Sangregorio, J. M. W. Seddon, E. Sinn, F. E. Sowrey, S. J. Teat, A. E. Terry, G. B. M. Vaughan and N. A. Young, *Chem. Eur. J.*, 2003, **921**, 5314-5322.

20 A. Tissot, C. Enachescu and M.-L. Boillot, *J. Mater. Chem.*, 2012, **22**, 20451.

21 S. Savage, Z. Jia-Long and A. G. Maddock, *J. Chem. Soc. Dalton Trans.*, 1985, 991-996.

22 P. Guionneau, *Dalton Trans.* 2014, **43**, 382-393; J. Tao, R-J. Wei, R. B. Huang and L. S. Zheng, *Chem. Soc. Rev.*, 2012, **41**, 703-737.

New Journal of Chemistry Accepted Manuscript

23 M. Marchivie, P.Guionneau, J.-F. Létard and D. Chasseau, *Acta Crystallogr.*, 2003, **59**, 479 ; J.-F. Létard, G. Chastanet, O Nguyen, S. Marcen, M. Marchivie, P. Guionneau, D. Chasseau and P. Gütlich, *Monatsh. Chem.,* 2003, **134**, 165.

24 M. A. Willard, L. K. Kurihara, E. E. Carpenter, S. Calvin and V. G. Harris, *Int. Mater. Rev.,* 2004, **49**, 125-170.

25 A. Hosseinian, S. Jabbari, A. R. Mahjoub and M. Movahedi, *J. Coord. Chem.,* 2012, **65**, 2623-2633.

26 N. Dragoe, M. Andruh and E. Segal, *Thermochimica Acta*, 1991, **176**, 241-248.

27 W. M. Reiff, R. B. Frankel, B. F. Little and G. J. Long, *Inorg. Chem.*, 1974, **13**, 2153 ; M. Wriedt and C. Näther I*norg. Chim. Acta* 2011, **377**, 129.

28 M. A. Halcrow, *Polyhedron*, 2007, **26**, 3523-3576.

29 K. F. Purcell and M. P. Edwards, *Inorg. Chem.*, 1984, **23**, 2620-2625.

30 E. König, K. Madeja and K. J. Watson, *J. Am. Chem. Soc.*, 1968, **90**, 1146.

31 S. Shi, G. Schmerber, J. Arabski, J.-B. Beaufrand, D. J. Kim, S. Boukari, M. Bowen, N. T. Kemp, N. Viart, G. Rogez, E. Beaurepaire, H. Aubriet, J. Petersen, C. Becker and D. Ruch, *Appl. Phys. Lett.*, 2009, **95**, 043303.

32 M. Cavallini, I. Bergenti, S. Milita, G. Ruani, I. Salitros, Z. R. Qu, R. Chandrasekar and M. Ruben, *Angew. Chem. Int. Ed.*, 2008, **47**, 8596.

33 M.-L. Boillot, J. Zarembowitch, A. Sour, In *Topics in Current Chemistry*; Gütlich, P., Goodwin, H. A., Eds.; Springer: Berlin, Germany, 2004; Vol. 234, p 261 ; A. Tissot, M.-L. Boillot, S. Pillet, E. Codjovi, K. Boukheddaden and L. M. Lawson Daku, *J. Phys. Chem. C*, 2010, **114**, 21715-21722.

New Journal of Chemistry Accepted Manuscript